

## The Diagnostic Potential of Transition Region Lines under-going Transient Ionization in Dynamic Events

J.G. Doyle<sup>1</sup> · A. Giunta<sup>2,3</sup> · A. Singh<sup>1,4</sup> ·  
M.S. Madjarska<sup>1</sup> · H. Summers<sup>2,3</sup> · B.J.  
Kellett<sup>3</sup> · M. O'Mullane<sup>2,3</sup> ·

© Springer ●●●

**Abstract** We discuss the diagnostic potential of high cadence ultraviolet spectral data when transient ionization is considered. For this we use high cadence UV spectra taken during the impulsive phase of a solar flares (observed with instruments on-board the *Solar Maximum Mission*) which showed excellent correspondence with hard X-ray pulses. The ionization fraction of the transition region ion O v and in particular the contribution function for the O v 1371 Å line are computed within the Atomic Data and Analysis Structure, which is a collection of fundamental and derived atomic data and codes which manipulate them. Due to transient ionization, the O v 1371 Å line is enhanced in the first fraction of a second with the peak in the line contribution function occurring initially at a higher electron temperature than in ionization equilibrium. The rise time and enhancement factor depend mostly on the electron density. The fractional increase in the O v 1371 Å emissivity due to transient ionization can reach a factor of 2–4 and can explain the fast response in the line flux of transition regions ions during the impulsive phase of flares solely as a result of transient ionization. This technique can be used to diagnostic the electron temperature and density of solar flares observed with the forth-coming Interface Region Imaging Spectrograph

**Keywords:** Sun: atmosphere – Sun: activity – Atomic processes – Line: formation

---

<sup>1</sup>Armagh Observatory, College Hill, Armagh BT61 9DG, N. Ireland email: jgd@arm.ac.uk

<sup>2</sup>Department of Physics, University of Strathclyde, 107 Rottenrow, Glasgow, G4 0NG, Scotland

<sup>3</sup>Space Science and Technology Department, STFC Rutherford Appleton Laboratory, Chilton, Didcot, Oxfordshire, OX11 0QX, UK.

<sup>4</sup>Dept.of Physics and Electronics, Deen Dayal Upadhyaya College, University of Delhi, India

---

## 1. Introduction

The solar atmosphere contains a range of highly dynamic features, e.g. flares, jets, spicules, etc. In order to fully observe these events, requires high cadence, high spatial and high spectral resolution instruments. However, due to various scientific and technical considerations, trade-offs in the instrument design must be made by the investigators. Milli-second data is commonly acquired in the radio and hard X-rays frequencies, while at ultraviolet wavelengths, high cadence is generally not available with most ultraviolet spectrographs. The highest cadence UV spectrometer to date was the Ultraviolet Spectrometer and Polarimeter (UVSP) which was flown on the *Solar Maximum Mission (SMM)* in the early 1980's. Several flares were observed simultaneously in the UV at selected individual spectral lines, e.g. O v 1371 Å, Si iv 1394 Å etc, and at hard X-ray energies of several keV. Several papers reported simultaneous (to within a fraction of a second) increases in the UV lines and at hard X-ray energies (Cheng *et al.* 1981, Woodgate *et al.* 1983, Poland *et al.* 1984, Cheng *et al.* 1984). A more in-depth study by Cheng *et al.* (1988) found that bursts observed in the O v 1371 Å line lagged the hard X-ray bursts by only 0.3 s to 0.7 s. No firm explanation was given for such a fast rise in the UV line flux.

None of the various spectrographs launched since SMM has had the ability to obtain high cadence spectral data. However, that will shortly change with the launch of the Interface Region Imaging Spectrograph (IRIS)<sup>1</sup> which is centered on four themes relating to solar physics and space weather, namely: Which types of non-thermal energy dominate in the chromosphere and beyond, how does the chromosphere regulate mass and energy supply to the corona and heliosphere and how does magnetic flux and matter rise through the lower atmosphere, and what role does flux emergence play in flares and mass ejections? The spectrograph will have the ability to obtain spectra with a cadence down to 1 s in several transition region line including the intense Si iv line at 1394 Å.

Such high cadence spectral data has the potential to provide diagnostic information on the plasma's electron temperature and density. To do so requires transient ionization considerations. As a test on the diagnostic potential we analyze one of the flares observed by SMM, making use of the Atomic Data and Analysis Structure (ADAS; Summers, 2009<sup>2</sup>) framework, which is a collection of fundamental and derived atomic data, and codes that manipulate them..

In Section 2, we briefly outline past observations and findings on the temporal and spatial correlation between HXR and UV emissions during solar flares and the high cadence UVSP data used in this paper, while in Section 3, we outline the atomic background, give details on a full time-dependent calculation and comparing it to the results obtained for the radiative power assuming steady state in Section 4. Here, we only consider an atomic model, i.e. we assume that the plasma is instantaneously heated from a cold plasma at  $2 - 3 \times 10^4$  K to temperatures  $3 - 5 \times 10^5$  K. We do not consider movement of plasma nor a model

---

<sup>1</sup><http://iris.lmsal.com/>

<sup>2</sup><http://www.adas.ac.uk>

---

atmosphere, as was done for comparison with jet-like features by Roussev *et al.* (2001), Doyle *et al.* (2002).

Most radiated power loss calculations are done on the basis of a steady-state ionization balance assumption, which is relatively simple and is often used in circumstances which are not fully justified. Non-equilibrium ionization occurs when the plasma electron temperature or electron density changes on a timescale,  $\tau_{plasma}$ , shorter than the atomic ionization stage fractional abundance relaxation timescale,  $\tau_z$  (where  $z$  is the ionization stage of a specific element), or when the time for plasma transport across a temperature or density scale length is shorter than  $\tau_z$ . In the present work, the first case is considered. Following McWhirter (1965), for an ionizing plasma,  $\tau_z$  represents the relaxation time for a plasma to reach ionization equilibrium. Transient ionization was considered by Doschek and Tanaka (1987) for  $20 \times 10^6$  K flare phase while Raymond (1990) looked at its effect for a micro-flare heated corona. In each instance, these authors noted a flux enhancement resulting from transient ionization considerations. Due to the general lack of high time resolution UV line flux observations, whether from flares or active regions, this aspect is not generally appreciated. In the present work the importance of non-equilibrium ionization is shown comparing the O v 1371 Å line emission enhancement (with respect to equilibrium) predicted by a model with the observation of a flare which occurred on 2 November 1980 (Poland *et al.* 1984).

## 2. Temporal and Spatial Correlation Between HXR and UV Emissions During Solar Flares

### 2.1. Past Observations

The relationship between HXR and UV emissions during flares has been investigated since the early 70s (Kane and Donnelly (1971) and references therein), using broadband EUV emission. Later Poland *et al.* (1984) and Cheng *et al.* (1981, 1988) found a strong temporal correlation between HXR emission at 25–100 keV and the O v 1371 Å emission, which peak at 25 eV ( $\approx 2.9 \times 10^5$  K), during the impulsive phase of solar flares. They used simultaneous observations obtained by the Hard X-Ray Burst Spectrometer (HXRBS) and Ultraviolet Spectrometer Polarimeter (UVSP) on the *Solar Maximum Mission (SMM)* satellite. The HXRBS had a temporal resolution of 0.128 s, but no spatial resolution, so it gave HXR emission from the entire Sun, while the O v emission was from the pixels showing flare enhancements. Poland *et al.* (1984) studied the temporal correlation between the HXR and O v emissions using a sample of 17 flares, finding a well defined relation between the two emissions for a given flare. However, this relation varies from one flare to the next. They analysed the observations in the context of a single loop model heated by a high-energy electron beam. The beam is accelerated down to the foot-points in the chromosphere. Here the beam collides with the cool chromospheric plasma and yields HXR bremsstrahlung emission, which heats the plasma through the Coulomb collision with the electrons. The plasma heated to transition region temperature

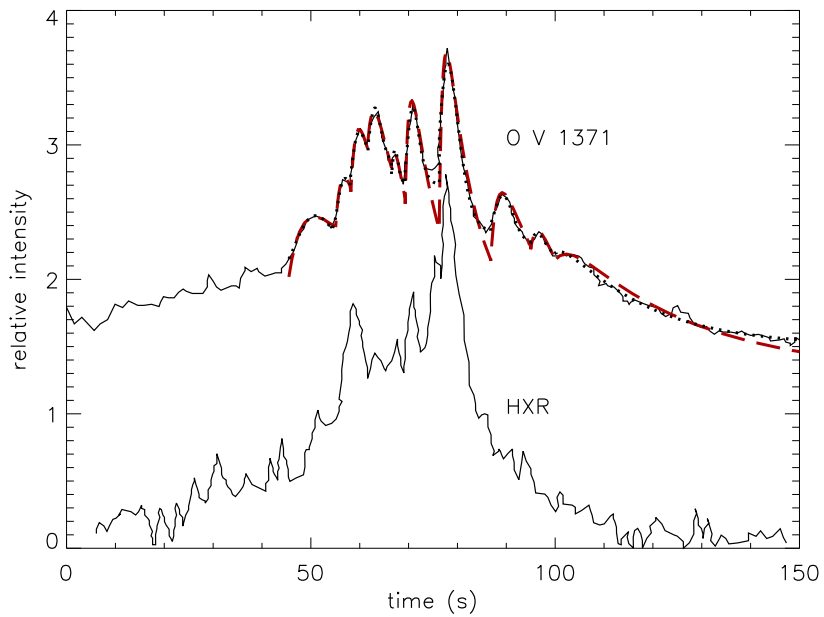
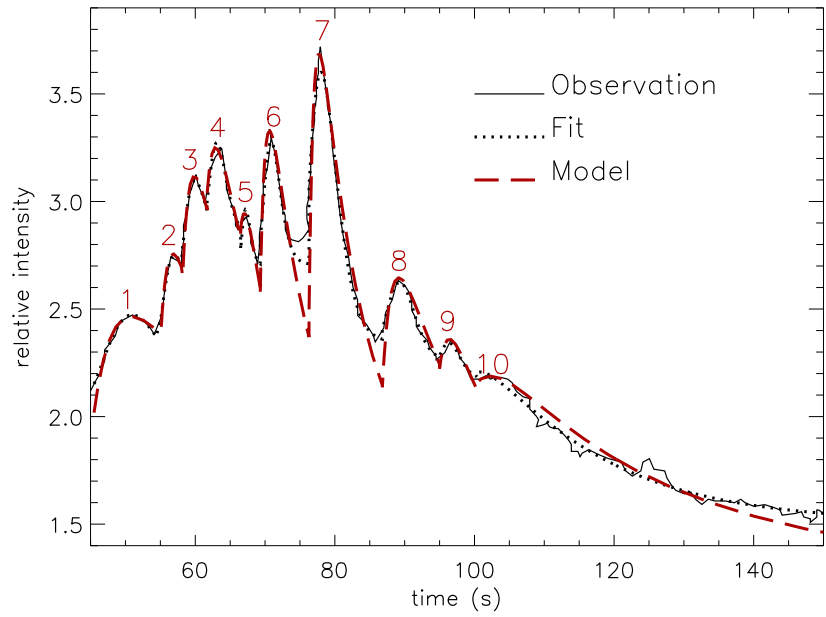


**Figure 1.** The UVSP and HXRBS data for a flare which occurred on 2 November 1980 (see Poland *et al.* 1984). The upper plot shows the O v 1371 Å light curve with the individual pulses labeled 1 to 10. The solid line represents the observation, the dotted line is the fit performed using the simple function given by Equation 6 and the red line is the sum of all the bursts (see Section 4). The lower plot displays the O v line light curve together with the hard X-ray emission to show the correlation between the O v bursts and the hard X-ray pulses.

---

gives increased O v emission. They concluded that there is a strong physical relationship between the processes which give rise to the non-thermal HXR emission and the apparently thermal UV emission. However, while they could predict with their models the general behaviour of O v emission compared to the HXR, they did not reproduce the magnitude and detailed behaviour. A close time correspondence between the HXR and O v emissions was found also by Cheng *et al.* (1988), who analysed five flare events. Their cross-correlation analysis showed that the fast features of O v generally lag behind the corresponding HXR features by 0.3-0.7 s. A revisit of the relationship between the UV and HXR emissions in flares was done by Warren and Warshall (2001). They studied nine flares, using data from it TRACE, it Yohkoh Hard X-Ray Telescope and Burst and Transient Source Experiment (BATSE) on the *Compton Gamma-Ray Observatory*, with a cadence of 2–3 s. For five of the nine flares their observations allowed the spatial analysis of the HXR sources (with a spatial resolution of 8''), finding for 2 flares a spatial separation between the HXR and UV sources. Further detailed studies on both temporal and spatial correlation between the HXR and UV emission in flares have been done by Alexander and Coyner (2006) and Coyner and Alexander (2009). They incorporated the improved spatial and temporal resolution of it TRACE (focusing on the 1600 Å observations) and RHESSI. The latter allows the examination of spatial HXR structures with a resolution of 2'', while it permits a time resolution of tens of milliseconds. However, the temporal analysis was limited by the it TRACE cadence of 2 s. They investigated the spatially integrated UV and HXR time profiles. In addition, they compared the individual UV sources (or group sources) with both the overall HXR time evolution and the individual impulsive X-ray bursts. Finally, they performed a spatial association between the spatial resolved UV and HXR sources. Alexander and Coyner (2006) focused on a particular flare, which occurred on 2002 July 16 and found a good temporal correlation between the spatially integrated UV and HXR emissions (as found by previous authors), but different temporal and spatial correlation for the individual sources. Three main conclusions arose from their work:

- (i) the strong overall correlation between the UV and HXR emissions suggests that these two different emissions must result from the same energy release process or a strictly related processes;
- (ii) the separation of the UV emission into individual sources provided examination of the various contributing components to the overall temporal behaviour and suggests a more complicated overall picture of solar flares than the single loop models of previous work;
- (iii) the lack of spatial correlation for some UV and HXR sources suggests a three-dimensional magnetic topology.

Coyner and Alexander (2009) improved the analysis of Alexander and Coyner (2006) investigating the behaviour of temporal and spatial UV and HXR emissions in a large sample of solar flares. They found that the HXR emission characterized by multiple impulsive bursts, that each individual burst corresponds to independent spatially disconnected sets of HXR foot-points. These sources are localized and are co-spatial with some of the UV sources. However, while the HXR sources are compact and localized, the UV emission is more

---

diffuse and persists throughout the entire flaring region. They noticed that some UV sources were not co-spatial but were co-temporal with respect to the HXR sources and some other UV sources showed neither co-spatial nor co-temporal emission compared to HXR sources. They explained the temporal but non-spatial correlation between some UV and the HXR sources, suggesting a three-dimensional magnetic field morphology, again more complex than single-loop models. Concerning the spatially and temporally uncorrelated UV emission, they pointed out that these signatures indicate two distinct types of UV response, one consistent with the HXR emission and one of a likely thermal origin (which may be indicated by the significant correlation with soft X-ray emission at 6-25 keV instead of the HXR at 25-100 keV). They concluded that in solar flares the structure of the magnetic field must be a complex three-dimensional structure and that there are multiple processes involved in the UV emission production. In summary individual bursts in the HXR time profile are related to disconnected sets of HXR foot-points and that a probable origin of the HXR emission is related to electrons (and ions) accelerated in the corona, traveling to the foot-points in the chromosphere. Here these electrons heat the plasma up to transition region temperature producing the UV emission.

There are three types of relationship between UV and HXR emission:

- (1) co-temporal and co-spatial UV and HXR emissions;
- (2) co-temporal but non co-spatial UV and HXR emissions;
- (3) neither co-temporal nor co-spatial UV and HXR emissions.

The first type of relationship, that is the existence of localized HXR emission co-spatial with temporally correlated UV emission sources, is consistent with models where both emissions result from different portions of an accelerated electron population. The second type of relationship, that is spatially separated but temporally correlated UV and HXR emissions, is consistent with a picture of a spatially complex magnetic geometry for solar flares, different from a single loop model. The third type of relationship, that is spatially and temporally uncorrelated UV and HXR emissions, is consistent with the presence of two distinct mechanisms each producing UV emission (e.g. one consistent with HXR origin and dependent on it and one of a likely thermal origin and independent of HXR emission).

## 2.2. The Data Used Here

The Ultraviolet Spectrometer and Polarimeter (UVSP) is described by Woodgate *et al.* (1980), while details on the Hard X-ray Burst Spectrometer (HXRBS) is given by Orwing *et al.* (1980). For the flare observations discussed here, the entrance aperture was  $10''$ , with an exit slit of  $0.3 \text{ \AA}$  centered at  $O \text{ v } 1371 \text{ \AA}$ . In response to an alert from another onboard instrument, the UVSP began making rasters covering  $30'' \times 30''$ . In some of the earlier UVSP/HXRBS flare observations, the UVSP data was taken with a 1.3 s cadence and in order to compare the two datasets, the UVSP data was interpolated at the finer HXRBS time resolution of 0.128 s. However, in most of the later observations, both datasets were observed using a 0.128 s cadence. In order to improve the S/N, several of the bright UVSP pixels were added.

---

Of the various papers which reported the almost simultaneous UV/hard X-ray bursts, Cheng *et al.* (1988) did a detailed filtering with a cross correlation analysis. These authors established that the O v 1371 Å line lagged the hard X-ray burst by 0.3 to 0.7 s, and was flare dependent. Here, we use this data to show the diagnostic potential of high cadence UV spectral data. In Fig. 1, we reproduce data from Poland *et al.* (1984) of a flare which occurred on 2 November 1980.

### 3. Atomic Background

To predict the line emissivities and ion population densities, the generalized collisional-radiative (GCR) theory as implemented in ADAS, the Atomic Data and Analysis Structure (McWhirter and Summers, 1984; Summers, 2009), is used in this work. Each ion in an optically thin plasma is described by a complete set of levels with collisional and radiative couplings between them. All radiative and electron collisional processes are included in the model, except for photon-induced processes. State-resolved direct ionization and recombination to and from the next ionization stage are also taken into account. In addition, due to the much shorter relaxation timescales for the excited states (not metastables) with respect to the ground and metastable states, it is assumed that the dominant populations lie in the ground and metastable states of the ion. Over the considered temperature and density regime, the ratio in the population of the metastable state  $2s2p^3P$  compared to the ground state  $2s^2^1S$  of O v is typically less than  $10^{-2}$ . Hence the dominant population is concentrated in the ground state.

In a time-dependent plasma model the line emissivity is no longer a unique function of the local temperature and density conditions but depends on the past history of the temperature, density and state of ionization of the plasma. Therefore, the assumption of ionization equilibrium in calculating the ionization balance is not appropriate and time-dependent fractional abundances must be determined. The time dependence of ionization stage populations,  $N^{(z)}$ , leads to the following equation:

$$\frac{dN^{(z)}}{dt} = N_e[S^{(z-1)}N^{(z-1)} + (S^{(z)} + \alpha^{(z)})N^{(z)} + \alpha^{(z+1)}N^{(z+1)}] \quad (1)$$

where the presence of metastable states is neglected because of the previous consideration.  $S$  and  $\alpha$  are the collisional-dielectronic ionization and recombination coefficients. They give the contribution to the growth rates for the ground state population, due to the effective ionization, which includes direct and excitation/auto-ionization contributions, and the effective recombination, which includes radiative, dielectronic and three-body contributions. The values of these coefficients, currently within the ADAS database, have been obtained following the GCR approach as described in Summers *et al.* (2006). The solution of Equation 1 is such that the number density of the element of a nuclear charge  $Z$ ,  $N^{(Z)}$ , is equal to  $\sum_{z=0}^Z N^{(z)}$ . The time-dependent fractional abundances  $N^{(z)}(t)/N^{(Z)}$  are calculated as follows: the code derives the solution for a range

---

of fixed plasma electron temperature and density pairs, starting from an initial population distribution  $N^{(z)}(t = 0)/N^{(Z)}$  (see Section 4) using an eigenvalue approach.

The line emissivity is given by:

$$\varepsilon_{j \rightarrow i} = A_{\text{el}} \frac{N_{\text{H}}}{N_{\text{e}}} N_{\text{e}}^2 G_{j \rightarrow i}^{(z)}(T_{\text{e}}, N_{\text{e}}, t) \quad (2)$$

where  $A_{\text{el}} = N^{(Z)}/N_{\text{H}}$  is the abundance of the element  $Z$  relative to hydrogen,  $N_{\text{H}}/N_{\text{e}}$  is tabulated by McWhirter *et al.* (1975) and  $G_{j \rightarrow i}^{(z)}(T_{\text{e}}, N_{\text{e}}, t)$  is the time-dependent contribution function defined as:

$$G_{j \rightarrow i}^{(z)}(T_{\text{e}}, N_{\text{e}}, t) = \mathcal{P}\mathcal{E}\mathcal{C}_{j \rightarrow i}^{(\text{exc}, z)} \frac{N^{(z)}(t)}{N^{(Z)}} + \mathcal{P}\mathcal{E}\mathcal{C}_{j \rightarrow i}^{(\text{rec}, z)} \frac{N^{(z+1)}(t)}{N^{(Z)}} \quad (3)$$

where

$$\mathcal{P}\mathcal{E}\mathcal{C}_{j \rightarrow i}^{(\text{exc}, z)} = A_{j \rightarrow i} \mathcal{F}^{(\text{exc}, z)} \quad (4)$$

$$\mathcal{P}\mathcal{E}\mathcal{C}_{j \rightarrow i}^{(\text{rec}, z)} = A_{j \rightarrow i} \mathcal{F}^{(\text{rec}, z)} \quad (5)$$

where  $A_{j \rightarrow i}$  is the transition probability  $N^{(z)}$  and  $N^{(z+1)}$  are the population densities of the ground states of the ions of charge  $z$  and  $z + 1$  and  $\mathcal{F}^{(\text{exc}, z)}$  and  $\mathcal{F}^{(\text{rec}, z+1)}$  are the effective contributions to the population of the upper excited state  $i$ . Further details on the GCR may be found in Lanza *et al.* (2001)

#### 4. Burst Model and Conclusions

The main goal of this work is the analysis of the effects of a plasma not being in ionization equilibrium due to rapid heating that is faster than the ionization/recombination timescales. The issue is addressed considering each burst (10 in this case, see Fig. 1) as an independent entity, which is assumed to originate as a consequence of a plasma heating at the foot of a loop in a multiple loop structure. Whether this energy release results from a non-thermal electron beam, and/or a conduction front is not the subject of this paper. The calculations performed for this work consider only the plasma response to sudden heating with no mass motions allowed.

Using the above considerations on the strong physical link between the HXR emission and the O v 1371 Å emission, the initial conditions for the plasma evolution are stated (see Table 1). For each burst it has been assumed that at time  $t = 0$ , the plasma is in ionization equilibrium at an electron temperature in the range  $3 - 5 \times 10^4$  K and the electron density in the range  $5 \times 10^{10} - 5 \times 10^{11} \text{ cm}^{-3}$  (typical values of the solar chromosphere). Using these initial conditions, the whole population of oxygen lies in the first four ionization stages (O I - O IV) and is concentrated essentially in the second and third ionization stages (O II and O III), as shown in Table 1. This Table lists only the range of the initial temperatures and densities considered because these initial conditions do



not significantly affect the late plasma evolution when the spectral lines observed are emitted. They depend strongly only on the final temperatures and densities. Then, to simulate a flare burst, the temperature of the plasma is instantaneously

**Table 1.** Initial conditions for the plasma evolution. At  $t = 0$  the fractional abundances have been calculated in equilibrium conditions, assuming  $T_e = 3 - 5 \times 10^4$  K and  $N_e = 5 \times 10^{10} - 5 \times 10^{11} \text{ cm}^{-3}$ . The table shows the fractional abundances for the most populated ionization stages in the stated  $(T_e, N_e)$  conditions.

$N_e \setminus T_e$	$3 \times 10^4$ K	$5 \times 10^4$ K
$5 \times 10^{10} \text{ cm}^{-3}$	O II=0.98	O II=0.28
	O III=0.01	O III=0.71
$5 \times 10^{11} \text{ cm}^{-3}$	O II=0.98	O II=0.25
	O III=0.01	O III=0.74

raised by a factor  $\approx 10$  (from around a few times  $10^4$  K to around a few times  $10^5$  K) with the bursts of Fig. 1 reconstructed following several steps, as listed below:

- (i) Each observed burst has been fitted using the function:

$$f(t) = N^{\text{ob}} B^R e^{-\left(\frac{t-t_S}{\tau^{\text{ob}}}\right)} \quad (6)$$

where  $B = (t - t_S)e^1 R^{-1} / \tau^{\text{ob}}$ ,  $\tau^{\text{ob}}$  is an exponential time decay,  $t_S$  is the start time of the burst,  $N^{\text{ob}}$  is the peak line enhancement value of the burst and  $R$  controls the width of the burst. This analytic expression has been used in the past in the context of the “smooth-burst model” (Doyle *et al.* 1991; Kellett and Tsikoudi (1999) and references therein) to estimate flare intensity profiles for different types of stars. Here this model has been used to reconstruct the profiles of the observed solar bursts and estimate their decay times ( $\tau^{\text{ob}}$ ) and peak values ( $N^{\text{ob}}$ ). Table 2 lists the values derived from this fitting procedure for each burst.

(ii) The modelled relaxation timescales,  $\tau^{\text{th}}$  of the ionization/recombination processes for O v have been calculated for different pairs of electron temperature and electron density using the relation given below (McWhirter, 1965). This relaxation time characterizes the time to reach ionization equilibrium and is defined as the reciprocal of the product of electron density and the sum of ionization and recombination coefficients relative to the considered ionization stages:

$$\tau^{\text{th}} = \frac{1}{N_e(S^{(z \rightarrow z+1)} + \alpha^{(z+1 \rightarrow z)})} \quad (7)$$

**Table 2.** Values of derived decay time ( $\tau^{ob}$ ) and peak line enhancement factor ( $N^{ob}$ ) for the ten observed bursts derived via fitting the function given in Section 4.

Burst	$\tau^{ob}$ (s)	$N^{ob}$
1	19.41	2.46
2	7.05	2.76
3	6.41	3.11
4	6.22	3.25
5	4.20	2.94
6	4.31	3.33
7	4.05	3.68
8	8.38	2.65
9	8.03	2.36
10	20.39	2.19

where  $z = 4$  is the ionization stage with which the O v 1371 Å line is concerned,  $S^{(z \rightarrow z+1)}$  denotes the effective ionization coefficient and  $\alpha^{(z+1 \rightarrow z)}$  the effective recombination coefficient.

(iii) A theoretical peak line enhancement factor value  $N^{th}$  represents the theoretical line enhancement at the peak of the burst with respect to the equilibrium value. An example is shown in Fig. 2. This figure plots the transient line contribution function  $G_{j \rightarrow k}^{tr}(T_e, N_e, t)$  as a function of time compared with the equilibrium line contribution function  $G_{j \rightarrow k}^{eq}(T_e, N_e)$  for two pairs of electron temperature and electron density values, which give the same  $\tau^{th}$  but different line enhancement factor  $N^{th}$ .

(iv) The theoretical relaxation timescales  $\tau^{th}$  and peak line enhancement factor values  $N^{th}$  have been derived for a set of  $(T_e, N_e)$  pairs for the calculation of the transient fractional abundances and equilibrium fractional abundances, respectively. Over-plotting contours with the observed values ( $\tau^{ob}$  and  $N^{ob}$ ) listed in Table 2, the final electron temperatures and electron densities for the time evolution of each burst are derived. Figure 3 displays an example for bursts 4 and 7. The lines with  $\tau$  constant (solid lines), corresponding to the decay times of the fourth and seventh bursts, intersect the lines with  $N$  constant (dashed lines), corresponding to the peak values of the two considered bursts. The intersection points give the electron temperatures and electron densities for the time evolution of these two bursts. The same procedure has been applied to the other bursts. The results are summarized in Figure 4, which shows a contour plot of the theoretical relaxation timescales as a function of electron temperature and electron density.

The over-plotted black lines are the contours which correspond to the observed decay times of Table 2. The white points represent the intersection with the

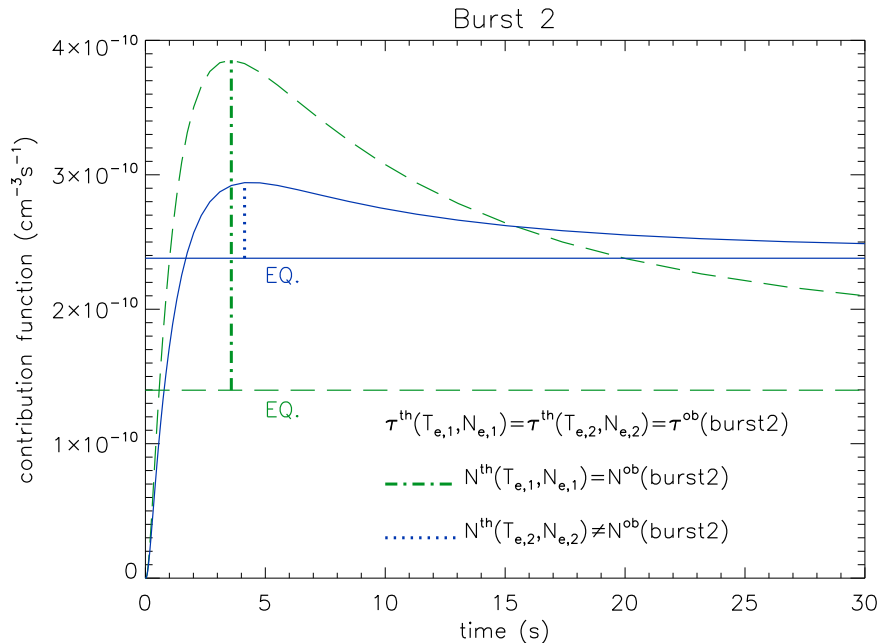


**Figure 2.** Contribution functions of O v 1371 Å as a function of time for reconstructing the second burst. The two solid straight lines are the equilibrium contribution functions calculated for two pairs of electron temperature and electron density values (the blue one is  $G_{j \rightarrow k}^{\text{eq}}(T_{e,1}, N_{e,1})$  while the green one is  $G_{j \rightarrow k}^{\text{eq}}(T_{e,2}, N_{e,2})$ ). The two curves which change with time represent the transient contribution functions calculated for the same two pairs of electron temperature and electron density. They are characterized by the same relaxation time  $\tau^{\text{th}} = \tau^{\text{ob}} = 7.05$  s but different peak values,  $N^{\text{th}}(T_{e,1}, N_{e,1}) = 2.76$  (which is equal to the observed value) and  $N^{\text{th}}(T_{e,2}, N_{e,2}) = 1.24$ .

$N$ -constant lines for each burst. The whole set of points lies in a region of quasi-constant electron temperature ( $T_e \approx 2.6 \times 10^5$  K), while there is a larger spread in the electron density domain ( $N_e \approx 2.6 \times 10^9 - 1.1 \times 10^{10} \text{ cm}^{-3}$ ), see also Figure 5. This figure shows that near to the highest peak (i.e. burst 7, Figure 1), the density is high while the relaxation time has one of the lowest values. The longest relaxation times are related to the first burst (burst 1) and last burst (burst 10). The latter is evidence of the slow decrease in the intensity of O v after the flare event due to the plasma relaxation until it reaches equilibrium conditions.

Figure 6 shows the contribution functions as a function of electron temperature. Note the much larger contribution function resulting solely from transient ionization. The dashed lines represent the instantaneous contribution functions calculated at the time where each burst peaks using the respective electron densities and the solid lines are the equilibrium contribution functions calculated at the same densities. The non-equilibrium contribution functions peak between  $2.6 - 2.9 \times 10^5$  K while the equilibrium contribution functions peak at  $2.1 \times 10^5$  K.

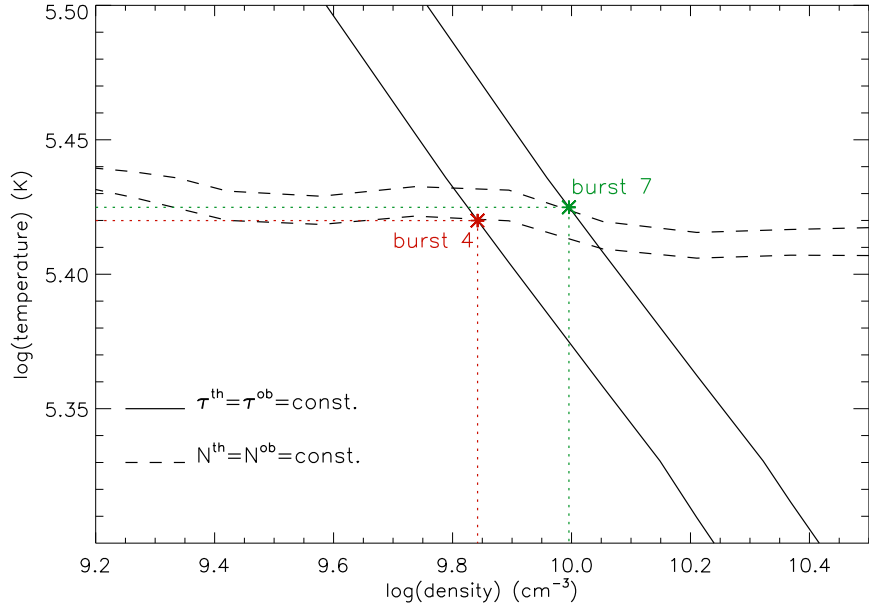


**Figure 3.** Lines with  $\tau$  constant (solid lines), corresponding to the decay times of the fourth and seventh bursts. The dashed lines have  $N$  constant, corresponding to the peak values of the two considered bursts. The intersection points give the derived  $T_e$  and  $N_e$

The final model to reconstruct the time evolution of each burst has been built up considering the following relation between the line emissivity calculated in non-equilibrium conditions at a fixed pair of electron temperature, and electron density and equilibrium line emissivity calculated for the same  $(T_e, N_e)$  pair:

$$\frac{\varepsilon_{j \rightarrow k}^{\text{tr}}(T_{e,i}, N_{e,i}, t)}{\varepsilon_{j \rightarrow k}^{\text{eq}}(T_{e,i}, N_{e,i})} = \frac{G_{j \rightarrow k}^{\text{tr}}(T_{e,i}, N_{e,i}, t)}{G_{j \rightarrow k}^{\text{eq}}(T_{e,i}, N_{e,i})} \quad i = 1, 2, \dots, 10 \quad (8)$$

where  $i$  is the burst number. Equation 8 provides the enhancement factor due to transient ionization with respect to the equilibrium conditions, see the red line in Figure 1 which is the sum of all the bursts.

In the previous section we used initial temperatures and densities typical of the solar chromosphere, in order to check the sensitivity of these values we performed additional calculations for one burst, in this instance burst 3. This burst showed an observed enhancement factor of about 3 and a decay time of about 6 s. It is possible to reproduce these values with a final  $N_e \approx 7 \times 10^9 \text{ cm}^{-3}$  and  $T_e \approx 2.6 \times 10^5 \text{ K}$ . Increasing the final temperature to  $1 \times 10^6 \text{ K}$  (with the initial temperature still in the range  $3 - 5 \times 10^4 \text{ K}$ ), and a final electron density in the range  $10^9$  to  $10^{13}$ , the enhancement factors becomes  $1 \times 10^5$  to  $1 \times 10^6$  instead of 3, while the decay times decreases from about 2 s to less than

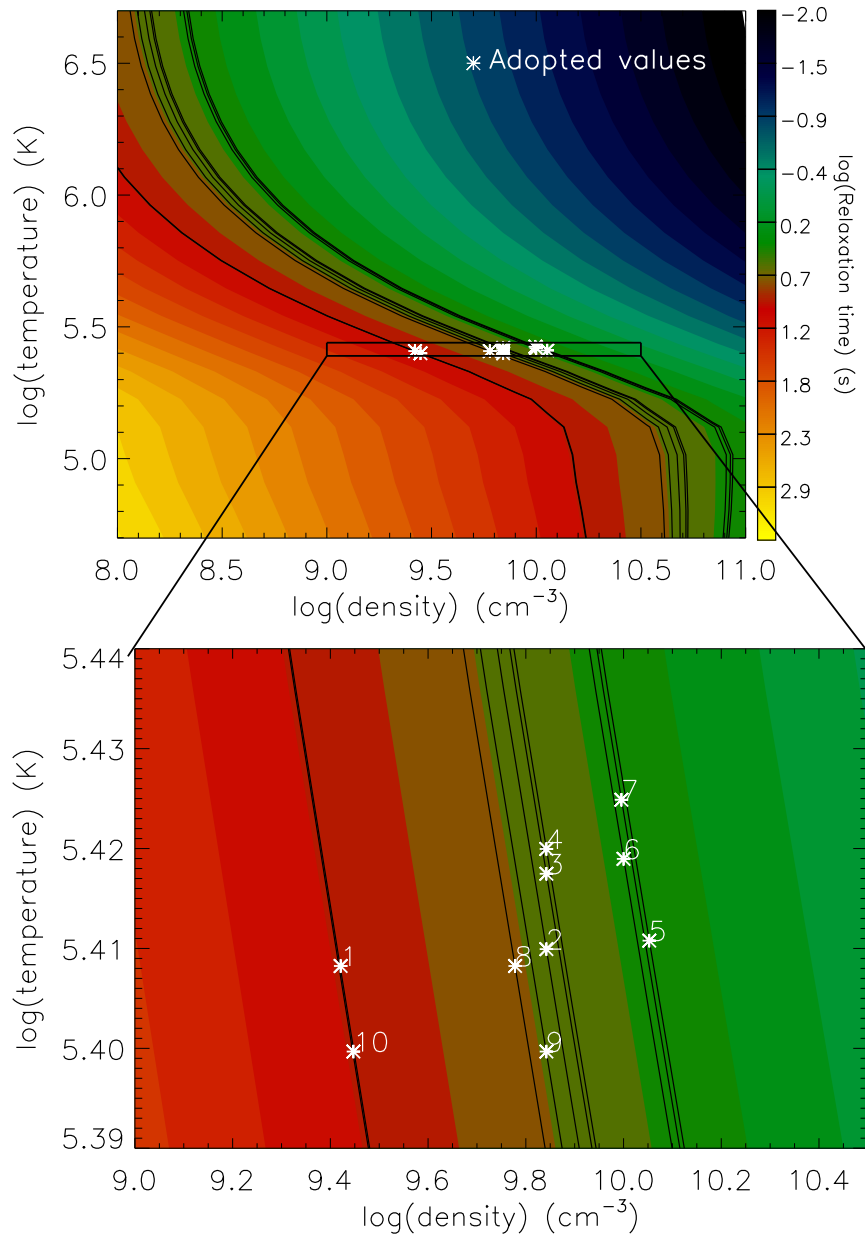


**Figure 4.** A contour plot of  $\tau^{\text{th}}$  calculated using Equation 7. The black lines are the constant  $\tau_s (= \tau^{\text{ob}})$  obtained by the fitting procedure. The white stars are the derived values of  $T_e$  and  $N_e$  for each burst, determined as in Fig. 3. The lower contour plot is an enlargement of the upper black rectangle showing the position of each burst labeled by numbers from 1 to 10.

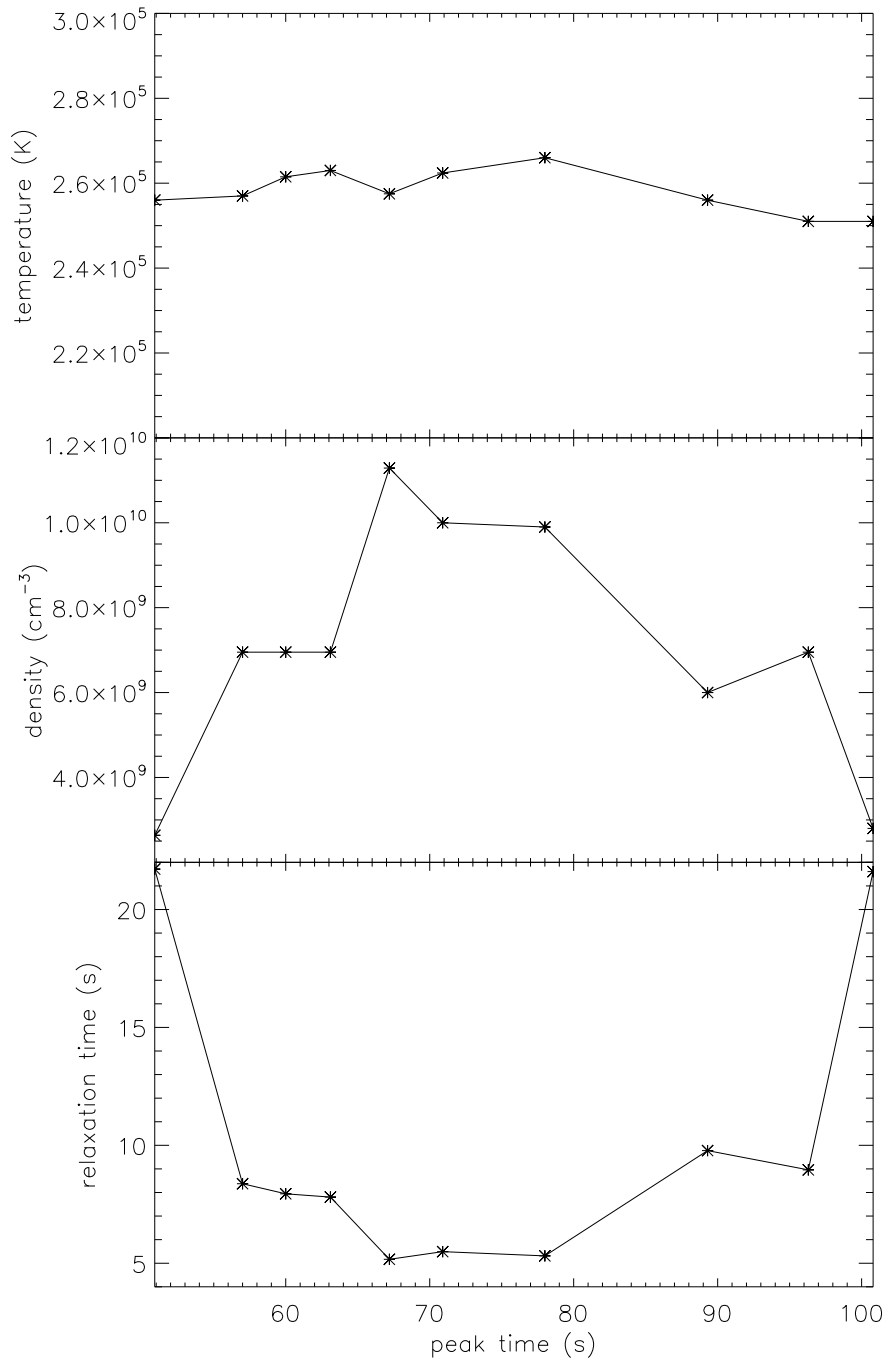


**Figure 5.** The derived electron temperature, electron density and relaxation time as a function of the time at which each burst has its peak.

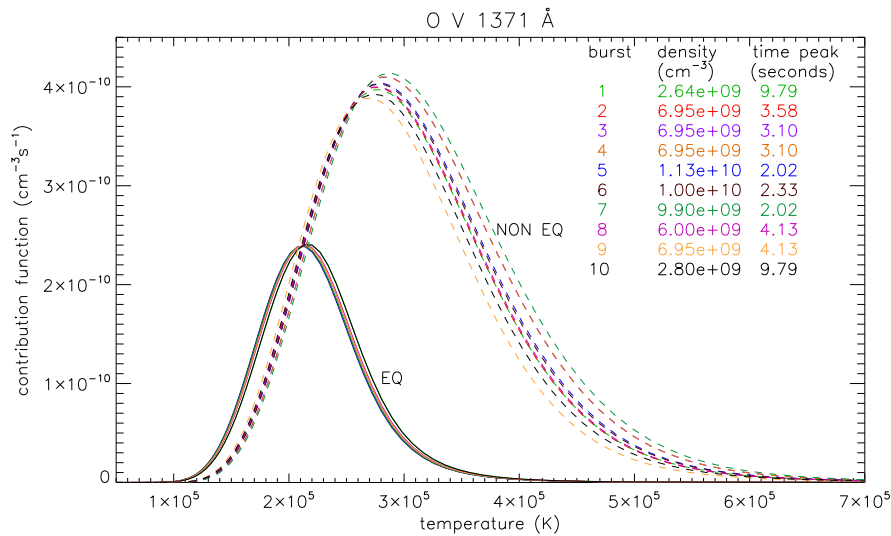


**Figure 6.** O v 1371 Å contribution functions as a function of electron temperature. The dashed lines are the instantaneous contribution functions at the time where each UV burst peaks. The corresponding electron density is given for each burst. The solid lines represent the contribution functions calculated using equilibrium ionization balance at the same electron density.

0.01 s as the density increases. Changing the initial temperature to  $1 \times 10^5$  K, only results in the final values changing by a few percentage. This means that in order to re-produce the observed enhancement and decay time, these initial conditions are appropriate.

The conclusion from the results given above is that even a small departure from ionization equilibrium can result in an enhancement of the O v 1371 Å line emission compared to the intensity calculated in ionization equilibrium. The present model reproduces the time evolution of each burst, although some issues need further investigation, e.g. it is noted that all the derived points in Fig. 4 lie in a very small temperature range. Thus more observations, together with a statistical analysis are needed to investigate whether this temperature behavior is the same for other flares.

This study assumes a Maxwellian electron distribution, which is justified by the substantially shorter average electron-electron energy relaxation time compared with the observed plasma development and with the theoretical ionisation stage (ground and metastables) relaxation times. However, the differential variation of electron-electron relaxation, especially to higher energies could allow a substantial cohort of fast electrons to confuse interpretation. It is unlikely that a sufficient set of line observations will be available for the solar atmosphere to explore this, however, it is hoped that parallel studies in tokamak divertor transients will clarify experimentally the non-Maxwellian spectral indicators.

What this work clearly shows is that observed transition region line intensity increases on a sub-second time-scale can be explained via transient

---

ionization. The response time is electron density dependent, explaining the reported O v/HXR time delays of Cheng *et al.* (1988). This work has implications not only for high cadence flare observations, but high cadence observations of other dynamic solar features (Doyle *et al.* 2006, Madjarska *et al.* 2009). There are currently no spectrographs capable of sufficiently high cadence observations, although the selected IRIS mission (launch date 2012) will be capable of obtaining such data for a range of transition region lines including Si IV 1394 Å and O IV 1401 Å. The contribution functions for these two lines behave differently theoretically under transient ionization, with Si IV 1398Å more like O v 1371Å. Both of these lines are in the ground state spin system. The O IV 1401Å line's upper state is in the quartet (metastable) spin system. Transient ionisation underfills the population structure of the alternate spin systems from the ground. By contrast the ground spin system population structure is enhanced with the exponential factors in the rate coefficients largely unwound because of the increased electron temperature.

**Acknowledgements** Research at the Armagh Observatory is grant-aided by the N. Ireland Dept. of Culture, Arts and Leisure. We thank STFC for support via ST/F001843/1 and ST/J00135X. MM and JGD thank the International Space Science Institute, Bern for the support of the team "Small-scale transient phenomena and their contribution to coronal heating".

## References

- Alexander, D. and Coyner, A.J.: 2006, *Astrophys. J.*, **640**, 505.
- Cheng, C.-C., Tandberg-Hanssen, E., Bruner, E.C., Orwig, L., Frost, K.J., Kenny, P.J., Woodgate, B.E. and Shine, R.A.: 1981, *Astrophys. J.* **248**, L39.
- Cheng, C.-C., Tandberg-Hanssen, E. and Orwig, L.E.: 1984, *Astrophys. J.* **278**, 853.
- Cheng, C.-C., Vanderveen, K., Orwig, L.E., and Tandberg-Hanssen, E.: 1988, *Astrophys. J.* **330**, 480.
- Coyner, A.J. and Alexander, D.: 2009, *Astrophys. J.* **705**, 554.
- Doscheck, G.A. and Tanaka, K.: 1987, *Astrophys. J.* **323**, 799.
- Doyle, J.G., Kellett, B.J., Byrne, P.B., Avgoloupis, S. Mavridis, L.N., Seiradakis, J.H., *et al.*: 1991, *Mon. Not. Roy. Astron. Soc.* **248**, 503.
- Doyle, J.G., Madjarska, M.S., Roussev, I., Teriaca, L. and Giannikakis, J.: 2002, *Astron. Astrophys.* **396**, 255.
- Doyle, J.G., Ishak, B., Madjarska, M.S., O'Shea, E. and Dzifčáková, E.: 2006, *Astron. Astrophys.* **451**, L35.
- Kane, S.R. and Donnelly, R.F.: 1971, *Astrophys. J.* **164**, 151.
- Kellett, B.J. and Tsikoudi, V.: 1999, *Mon. Not. Roy. Astron. Soc.* **308**, 111.
- Lanza, A.F., Spadaro, D., Lanzafame, A.C., Antiochos, S.K., MacNeice, P.J., Spicer, D.S. and O'Mullane, M.G.: 2001, *Astrophys. J.* **547**, 1116.
- Madjarska, M.S., Doyle, J.G., and De Pontieu, B.: 2009, *Astrophys. J.* **701**, 253.
- McWhirter, R.W.P.: 1965, p201, In: Huddleston, R.H., Leonard, S.L. (eds.) "Plasma Diagnostic Techniques", *Academic Press New York*.
- McWhirter, R.W.P., Thonemann, P.C. and Wilson, R.: 1975, *Astron. Astrophys.* **40**, 63.
- McWhirter, R.W.P. and Summers, H.P.: 1984, 'Applied Atomic Collision Physics, Volume 2: Plasmas. Edited by C.F. Barnett and M.F.A. Harrison. ISBN 0-12-478802-5. Published by Academic Press, New York: 1984, p.52–111.
- Orwig, L.E., Frost, K.J. and Dennis, B.R.: 1980, *Solar Phys.* **65**, 250.



- 
- Poland, A.I., Orwig, L.E., Mariska, J.T., Nakatsuka, R. and Auer, L.H.: 1984, *Astrophys. J.* **280**, 457.
- Raymond, J.C.: 1990, *Astrophys. J.* **365**, 387.
- Roussev, I., Doyle, J.G., Galsgaard, K. and Erdelyi, R.: 2001, *Astron. Astrophys.* **380**, 719.
- Summers, H.P. and Hooper, M.B.: 1983, *Plasma Phys.*, **25**, 1311.
- Spitzer, L.: 1962, p120, *Physics of Fully Ionized Gases*, New York, Interscience (2nd edition).
- Summers, H.P., Dickson, W.J., O'Mullane, M.G., Badnell, N.R., Whiteford, A.D., Brooks, D.H., Lang, J., Loch, S.D. and Griffin, D.C.: 2006, *Plasma Phys. and Controlled Fusion*, **48**, 263.
- Summers, H.P.: 2009 *The ADAS User Manual*, <http://www.adas.ac.uk/manual.php>.
- Warren, H.P. and Warshall, A.D.: 2001, *Astrophys. J.* **560**, L87.
- Woodgate, B.E., Brandt, J.C., Kalet, M.W., Kenny, P.J., Tandberg-Hanssen, E.A., Bruner, E.C., Beckers, J.M., Henze, W., Knox, E.D. and Hyder, C.L.: 1980, *Solar Phys.* **65**, 73.
- Woodgate, B.E., Shine, R.A., Poland, A.I. and Orwig, L.E.: 1983, *Astrophys. J.* **265**, 530.

